physics

MDPI

Article

Electron Beam Transport in Plasma-Accelerator-Driven Free-Electron Lasers in the Presence of Coherent Synchrotron Radiation and Microbunching Instability

Simone Di Mitri [1,2,*] **and Giovanni Perosa** [2]

[1] Elettra—Sincrotrone Trieste S.C.p.A., 34149 Basovizza, Italy
[2] Department of Physics, University of Trieste, 34100 Trieste, Italy; giovanni.perosa94@gmail.com
* Correspondence: simone.dimitri@elettra.eu

Received: 26 August 2020; Accepted: 26 September 2020; Published: 30 September 2020

Abstract: Laser- and beam-driven plasma accelerators promise electron beam brightness at the exit of plasma cells suitable for X-ray free-electron lasers. Beam transport from the accelerator to the undulator may include a multi-bend, energy-dispersive switchyard, in which energy collimators can be installed to protect the undulator or to serve multiple photon beamlines. Coherent synchrotron radiation and microbunching instability in the switchyard can seriously degrade the brightness of the accelerated beam, reducing the lasing efficiency. We present a semi-analytical analysis of those collective effects for beam parameters expected at the exit of state-of-the-art plasma accelerators. Prescriptions for the linear optics design used to minimize transverse and longitudinal beam instability are discussed.

Keywords: electron beam collective effects; free-electron laser; linear optics

1. Introduction

The rapid development of narrow-bandwidth free-electron lasers (FELs) has drawn the attention of the particle accelerator community to the spectral degradation that originates from the microbunching instability (MBI) [1,2]. This instability results from the interplay of the longitudinal space charge (LSC) force at the micron scale [3], emission of coherent synchrotron radiation (CSR) [4,5], and the energy dispersion function in multi-dipole magnetic insertions, such as magnetic compressors and switchyard lines. MBI is exhibited as broadband density and energy modulation at wavelengths comparable to those involved in the FEL coherent emission. Such modulations in the beam longitudinal phase space can enlarge the intrinsic FEL bandwidth via sideband instability [6]. Additionally, if the associated large slice energy spread (SES) [7] exceeds the FEL normalized energy bandwidth, the FEL output peak power is reduced, the saturation length is lengthened, and as a result the FEL brilliance is degraded for any given undulator length.

The development of FEL projects at short wavelengths has occurred in parallel to the growing interest and rapid progress in laser- and beam-driven, plasma-based accelerators, whereby high-quality electron beams can be accelerated to multi-GeV energy levels in centimeter-scale plasma [8–14]. If carefully manipulated, such beams can exploit 6-dimensional brightness suitable for lasing. Endeavors to accelerate electron beams beyond several GeV are underway worldwide at large-scale laser and particle accelerator facilities.

In FEL facilities driven by plasma accelerators, the MBI can be originated in a multi-bend switchyard line downstream from the acceleration stage. A switchyard is adopted to install energy collimators to protect the undulator or to serve multiple photon beamlines [15–20]. However, some differences with respect to the transport of high-brightness beams driven by radiofrequency (RF) accelerators

should be pointed out. First, an electron beam exiting a plasma cell is not subject to the longitudinal beam gymnastics that are commonly adopted in magnetic compressors, because the plasma accelerator already provides multi-kA peak current bunches. Second, the path length to reach the undulator in RF linacs along which the LSC force develops is dominated by the linac length, typically spanning from 0.1 to 3 km for final beam energies in the range of 1–17 GeV [21]. In plasma-based accelerators, the beam can instead exit the plasma cell at beam energies already suitable for lasing in soft X-rays (e.g., 1 GeV or more). In such cases, the effect of the LSC is basically limited to the switchyard, whose maximum total length can be estimated at several tens of meters for multi-GeV beam energies. Third, the longitudinal phase space generated by plasma accelerators usually shows large relative SES values in the range of approximately 0.1–1% [22–25], which tends to dampen the MBI by virtue of Landau energy damping before any amplification builds up, as shown below. In summary, by virtue of the compact footprint of a plasma accelerator, the MBI is expected to be alleviated compared to RF linacs. Nevertheless, in spite of lower bunch charges, the beam charge density in plasma accelerators can still be very high. Moreover, schemes for the reduction of the SES at the entrance of the undulator are being pursued to achieve more efficient lasing [26–30]. Since the MBI gain is proportional to the bunch peak current and inversely proportional to the transverse beam sizes, and since Landau damping becomes less effective for low SES values relative to the beam energy, it is worth paying attention to the growth of the instability in the switchyard line downstream of a plasma accelerator, which is the motivation for the present study.

The challenge of beams transported from the exit of a GeV-class plasma accelerator to an undulator for coherent emission has been touched on in the above reported literature from different perspectives. However, the impacts of collective effects, such as from CSR and LSC, in a dispersive transfer line, with special attention paid to the use of multi-GeV beams for lasing in X-rays, has not been investigated yet. Moreover, we conduct this study with a semi-analytical modeling approach for MBI as introduced in [31], in light of a recently revisited theory of intra-beam scattering (IBS) for single-pass systems [32]. The instability is characterized in terms of the spectral contents of density and energy modulations and the equivalent SES. This approach is expected to capture the physics of MBI and to allow fast optimization of the beam delivery system. On the contrary, massive particle tracking would provide details of the 6-dimensional particle distribution, which is outside of the capability range of the semi-analytical model, but at the expense of far larger computational requirements.

Because of the uncertainty of the uncorrelated energy spread at the exit of the plasma cells, which may strongly depend on the details of the scheme adopted for beam generation and acceleration, we will consider this as a variable. The MBI in the switchyard is, thus, analyzed as a function of the momentum compaction or longitudinal transport matrix term (R_{56}) of the line, while for the initial uncorrelated energy spread in the range of 10–300 keV, beam energies of 1 and 5 GeV are considered. While the root-mean-square (RMS) value of the total energy spread of the plasma-accelerated beam could be 1%, which is commonly the case when non-linear correlations in the beam's longitudinal phase space appear, the slice energy spread (SES) (i.e., the energy spread evaluated along a short portion of the bunch, for example the slice duration < fs) could be much smaller [30]. The case of SES ~100 keV at 1 GeV beam energy reflects state-of-the art manipulation of the electron beam before entering the undulator. Lower SES values of tens of keV are most likely out of the present scope of plasma accelerators. The aim of this paper is two-fold: to point out potential showstoppers in lasing due to the MBI in cases of super-cold beams, as specified in [30]; to mimic a stronger source of instability at the entrance of the switchyard due to causes such as pre-bunched beams (either in terms of the energy or density, or both). Finally, the highest energy of 5 GeV is used to identify any scaling of the instability strength and of the optics prescriptions used to counteract it with beam energy. As will be shown in the following section, the considered range of parameters allows one to capture the trend of the instability growth or mitigation, so that the physics of the instability at either smaller or larger values of the energy spread can be easily inferred from our findings.

The MBI is a longitudinal collective beam effect, which receives contributions from both the LSC and CSR. The latter can also lead to intolerable projected emittance growth in the bend plane. As a follow up to the MBI study, we provide analytical prescriptions for the terms of the first-order transport matrix of the switchyard, which are necessary conditions—although are not sufficient—for the preservation of the bend plane emittance in the presence of CSR kicks.

2. Model of Microbunching Instability

2.1. Electron Beam Delivery System

We consider the electron beam parameters at the exit of a plasma accelerator, which are similar to those in the Eupraxia proposal [33] (see Table 1). The same set of parameters is assumed at energy levels of 1 and 5 GeV. A ~30-m long switchyard made of two double-bend cells is considered (see Table 2). The presence of several quadrupole magnets distributed along the switchyard is assumed, which allows variable momentum compaction (from positive to null to negative values) by means of a distributed energy dispersion function. Overall, the line is assumed to be achromatic at the first order. On the one hand, a higher beam rigidity at 5 GeV corresponds to weaker LSC and CSR effects on the beam energy distribution. On the other hand, since the switchyard footprint and the dipole bending angle are kept fixed, a stronger CSR field is expected by virtue of a stronger dipole field. At this stage, we assume that any residual correlation in the longitudinal phase space at the scale of the bunch length is small enough to cause any variation in the bunch duration, and therefore in the peak current, to be negligible. The validity of this assumption, however, will be verified and discussed later on, where tolerances of the total beam energy spread (including correlations in the phase space), or equivalently the switchyard transverse and longitudinal dispersion functions, will be given.

Table 1. Electron beam parameters at the exit of the plasma accelerator.

Parameter	Value
Energy	1, 5 GeV
Charge	30 pC
Peak current	3 kA
Duration, RMS	4 fs
Slice energy spread, RMS	10–300 keV
Normalized emittance, RMS	0.3 μm rad
Transverse size, RMS	<40 μm

Table 2. Parameters of a switchyard made of two double-bend cells.

Parameter	Value
Energy	1, 5 GeV
Dipole length	0.5 m
Dipole bending angle	5, 3 deg
Drift length in each cell	5 m
Drift length between cells	10 m
$\lvert R_{56}\rvert$	<3 mm
Maximum dispersion function	30 mm
Average betatron function	10 m

2.2. Spectral Gain and Slice Energy Spread

The MBI is modeled via the Bosch–Klemann semi-analytical approach [31]. The instability is analyzed from the exit of the plasma cell to the switchyard end, which includes the IBS values evaluated for single-pass systems [32]. The model is able to follow the coupled dynamics of density and energy modulations, i.e., the successive transformation of density modulations into energy modulations through LSC and CSR, and of energy modulations into density modulations via R_{56}.

In order to estimate the impact of the MBI on the FEL spectral bandwidth, we assume lasing in the soft X-ray wavelength range of 0.5–5 nm. The FEL parameter ρ_{FEL} [34], which is associated with this wavelength range and with the electron beam parameters in Table 1, is in the range of 0.03–0.06%. The FEL longitudinal coherence length can be estimated as $\lambda_{\mathrm{FEL}}/(4\pi\rho_{\mathrm{FEL}})$, i.e., at the sub-micron level, where λ_{FEL} is the lasing wavelength. We conclude that although the instability is naturally broadband, only modulation periods in the range of ~0.1–10 μm are expected to have a substantial impact on the lasing. We, therefore, collapse the information for the "strength" of the instability into the spectral integral of the energy modulation curve in the aforementioned bandwidth, which is weighted by the instability gain [7,32]. We refer to this quantity as σ_{MBI}. If the instability is weak, or if it peaks at wavelengths much shorter than the FEL longitudinal coherence length, σ_{MBI} can be interpreted as an effective SES. Although the calculated σ_{MBI} cannot be used to quantitatively predict the FEL spectral purity, the weaker the instability gain, the lower the σ_{MBI} is, and the smaller the amount of FEL energy expected to be dispersed into sidebands.

The σ_{MBI} is calculated by integrating the CSR- and LSC-induced energy modulation, $\Delta\gamma(\lambda)$, over a specific range of modulation wavelength λ. This is the product of the Fourier transform of the initial current distribution with the average value I_0 or bunching factor $b_0(\lambda)$, the instability amplification factor or gain $G(\lambda)$, and the Fourier transform of the collective effect or impedance $Z(\lambda)$. The initial bunching is defined with a broadband shot-noise-like spectral distribution of bandwidth $\Delta\nu$:

$$\left|b_0(\lambda)\right|^2 = \frac{2e}{I_0}\Delta\nu = \frac{2ec}{I_0}\frac{\Delta\lambda}{\lambda^2}, \tag{1}$$

where e is the electron charge and c the light speed in vacuum.

The gain, i.e., the ratio of the final and initial bunchings, is [3,35,36]:

$$G(k) \cong \frac{4\pi I_0}{Z_0 I_A} Ck|R_{56}|\left|\int ds \frac{Z(k;s)}{\gamma(s)}\right| \exp\left[-\frac{1}{2}(CkR_{56}\sigma_\delta)^2\right], \tag{2}$$

where $Z_0 = 376.73\ \Omega$ is the vacuum impedance, $I_A = 17{,}045$ A is the Alfven current, $r_b = 0.8735\left(\sigma_x + \sigma_y\right)$ is the effective electron beam radius calculated as function of the average RMS tranverse beam sizes σ_x and σ_y; I_1, K_1 are modified Bessel functions of the first kind; C is the bunch length compression factor (=1 in our case); $k = 2\pi/\lambda$ is the modulation wavenumber; and σ_δ is the relative uncorrelated energy spread at the entrance of the beam line. The integral is over the variable s, i.e., the longitudinal coordinate along the beam line. The resulting energy modulation amplitude is:

$$\left|\Delta\gamma(\lambda)\right|^2 = \left|G(\lambda)b_0(\lambda)Z_{\mathrm{int}}(\lambda)\right|^2, \tag{3}$$

with $Z_{\mathrm{int}}(\lambda)$ being the impedance integrated over the beam line length. The equivalent RMS energy spread is the integral of the modulation amplitude over the whole spectrum of modulations (or part of it). By substituting Equation (1) into Equation (3), we find:

$$\sigma^2_{\mathrm{MBI}} = \int \left|\Delta\gamma(\lambda)\right|^2 = \frac{2ec}{I_0}\int d\lambda \frac{\left|G(\lambda)Z_{\mathrm{int}}(\lambda)\right|^2}{\lambda^2}. \tag{4}$$

The IBS-induced energy spread modifies the exponential term of the gain in Equation (2) (Landau damping). The gain in successive dispersion regions of the beam line is, therefore, diminished, with an overall mitigation effect on the instability. It was shown in [32] that in configurations of high gain (e.g., $G > 100$), neglecting the IBS contribution to σ_δ can lead to unrealistic predictions of the instability, and in particular of the final energy spread. The energy spread in Equation (4) is summed by quadrature to the uncorrelated energy spread of the unperturbed beam and to that induced by IBS. The results are compared for different optics settings of the switchyard line, together with the spectral behavior of the density and energy gain.

2.3. Switchyard Optics Design

Theoretical and experimental studies [37–39] have indicated that the FEL sideband instability can be mitigated by tuning the R_{56} of the switchyard to an isochronous condition (henceforth, $R_{56} = 0$). The solution $R_{56} = 0$ is built by following the prescriptions for minimization of the CSR-induced microbunching, i.e., the beam line has to be globally and locally isochronous. We model this condition by imposing $R_{56} = 0$ at the exit of each double-bend cell of the switchyard. Moreover, sub-mm (absolute) deviations of the local R_{56} are imposed at the exit or entrance of the dipole magnets. This strategy aims to minimize the term [37]:

$$\xi = \left| \max\left\{ R_{56}^{s' \to s} \right\} \frac{k^{1/3}}{\rho^{2/3}} \Delta L \right| \tag{5}$$

which is able to drive the CSR instability in a multi-bend line. $R_{56}^{s' \to s}$ is the value of R_{56} evaluated at consecutive dipole locations s' and s along the beam line, ρ is the dipole bending radius, and $\Delta L = s' - s$.

However, if either the beam is pre-bunched at the entrance of the switchyard or the LSC impedance accumulated over the whole line has a substantial contribution to the overall gain, a non-isochronous switchyard optics might give the best conditions for suppressing the instability [39]. This is because the accumulated energy modulation translates into an effective longitudinal position–energy correlation at the modulation wavelength (the local "chirp") [40]. A longitudinal slippage of particles, or phase mixing, is generated by the non-zero R_{56} multiplied by the local energy chirp, which smoothens the beam's longitudinal phase space. This translates into a red shift of the instability peak gain towards wavelengths that no longer interfere with the FEL natural bandwidth. It is worth noting that contrary to Landau energy damping, the effect of phase mixing depends on the sign of R_{56}.

3. Results

3.1. Microbunching Instability

Figure 1 shows the spectral energy modulation, bunching factor, and gain for three optics settings of the switchyard line at 1 GeV for an initial energy spread of 10 keV RMS. This low energy spread corresponds to the scenario with the strongest MBI because of the limited Landau damping, which allows us to input evidence of the impacts of linear optics on the instability gain. The initial bunching factor is calculated from Equation (1), which amounts to ~10^{-6} at the wavelength of 10 nm. The scenario with $R_{56} > 0$ corresponds to individually achromatic double-bend cells (the R_{56} value of a 4-dipole chicane is negative with this convention). The isochronous condition has been discussed in Section 2.3, and it assumes a distributed energy dispersion function through the whole line. Optics with $R_{56} < 0$ can also be produced with a distributed energy dispersion function through the line, where larger values of the dispersion are expected at the dipoles' location. Table 3 lists the peak gain and σ_{MBI} predicted by the model for each optics setting. A systematic investigation of σ_{MBI} as a function of the initial energy spread reveals that IBS leads to a <10% reduction of the peak gain only for the initial absolute RMS energy spread $\sigma_{E,i} \leq 20$ keV. Figure 2 summarizes the trend of the σ_{MBI} (final SES) as a function of $\sigma_{E,i}$ for the three optics.

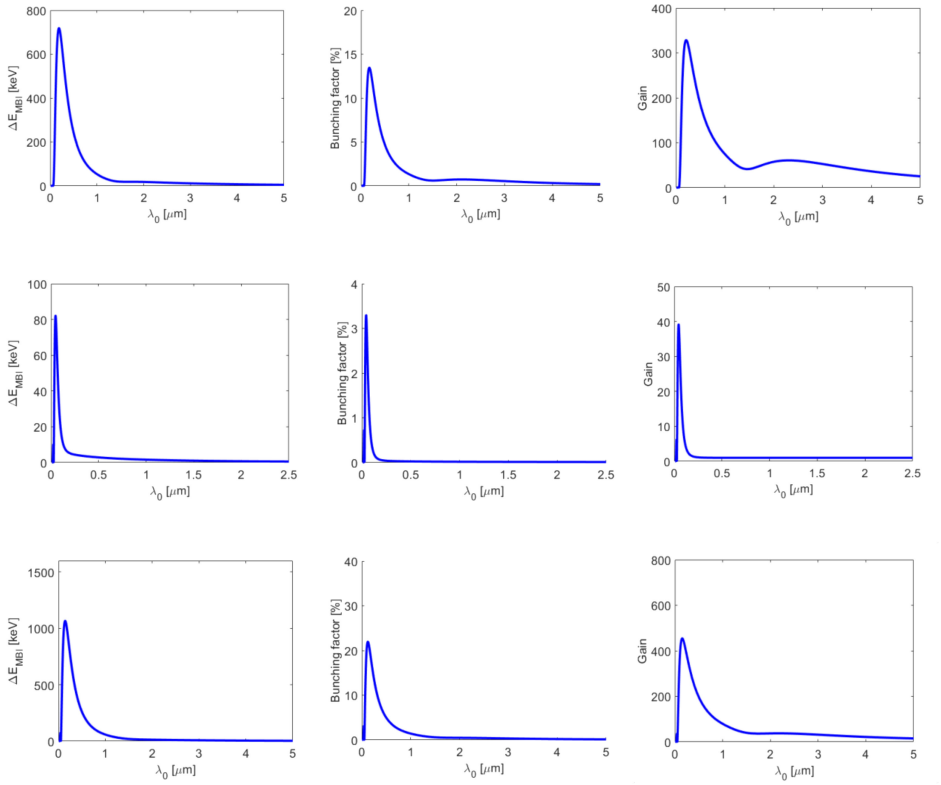

Figure 1. From left to right are the final energy modulation, bunching factor, and gain as a function of the initial modulation wavelength λ_0. For the longitudinal transport matrix term R_{56} = –2.5 mm (**top**), 0 (**middle**), and +2.5 mm (**bottom**), respectively. We note the different scales used for the three cases.

Table 3. The calculated peak gain and final slice energy spread (SES, also σ_{MBI} in the text) for the three values of the longitudinal transport matrix term R_{56} of the switchyard for 1 GeV beam energy and 10 keV initial energy spread.

R_{56} [mm]	Peak Gain	σ_{MBI} [keV]
+2.5	407	928
0	38	64
−2.5	281	565

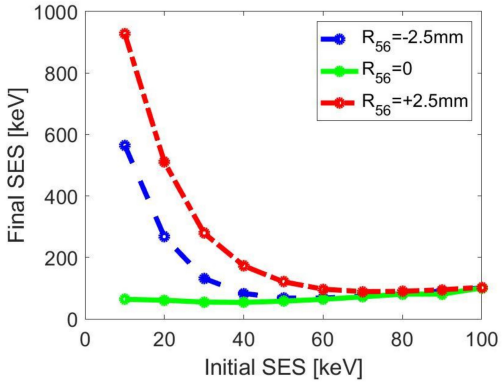

Figure 2. The calculated final slice energy spread (SES, also σ_{MBI} in the text) vs. initial slice energy spread for three switchyard optics (also see Table 3).

3.2. Coherent Synchrotron Radiation

The CSR tail–head instability causes projected emittance growth in the bend plane [41]. We have so far assumed that for any value of R_{56}, the switchyard optics are flexible enough to allow cancellation of CSR kicks [42]. This implies small bend plane betatron functions at the dipoles' location and π-betatron phase advances between the dipoles. The cancellation of successive CSR kicks is effective if the bunch length does not change considerably from dipole to dipole. Specifically, the quantity $R_{56}\sigma_{E,i}/E$ must be much smaller than the bunch length. Additional contributions to the bunch length variation come from the products $R_{51}\sigma_{x,i}$ and $R_{52}\sigma_{x\prime,i}$ at the first order, with $\sigma_{x,i}$ and $\sigma_{x\prime,i}$ being the beam size and angular divergence at the entrance of the switchyard, respectively. For the normalized beam emittance of $\varepsilon_x \cong \gamma\sigma_{x,i}\sigma_{x\prime,i} = 0.3$ μm rad, 1 GeV beam energy, and initial energy spread in the range of $\sigma_{E,i} = 30$–300 keV, the maximum values of transport matrix terms R_{51}, R_{52}, and R_{56} (coupling the final longitudinal particle coordinate internal to the bunch to, respectively, the initial horizontal position, horizontal angular divergence and relative energy deviation) along the switchyard are calculated by assuming a maximum tolerable bunch length variation of 10% or 0.1 μm. The results are shown in Figure 3 as functions of the beam size and energy spread at the entrance of the switchyard.

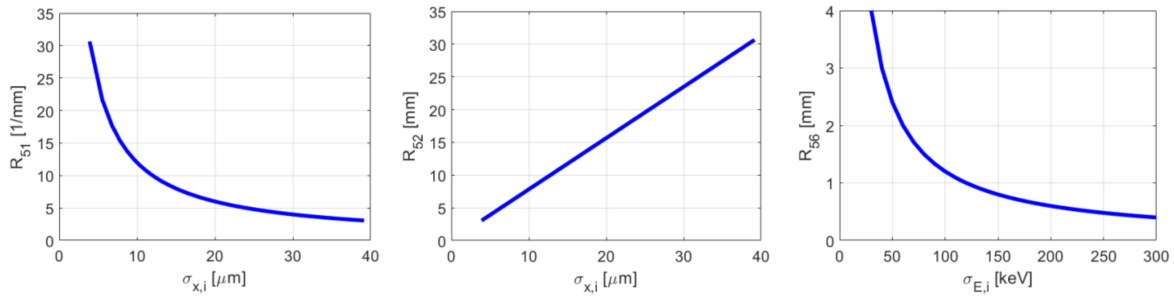

Figure 3. Maximum values for R_{51},R_{52}, and R_{56} along the switchyard for a maximum bunch length variation of 0.1 μm as functions of the initial beam size and energy spread at the beam energy level of 1 GeV.

4. Discussion

The semi-analytical estimation of the MBI through the switchyard indicates that the isochronous optics minimize the instability with respect to both positive and negative momentum compaction. The reduction in the peak gain and peak energy modulation amplitude is up to 10-fold (see Figure 1). However, the isochronous optics blue shifts the maximum gain at sub-μm wavelengths, which could still interfere with lasing at < 1 nm. We, therefore, assess the effective suppression of the instability by calculating the final effective slice energy spread vs. the initial one (see Figure 2). In doing so, we find that the optics associated with a larger gain, i.e., non-zero R_{56}, show a non-linear trend of σ_{MBI} for $\sigma_{E,i} < 60$ keV, which is a signature of the phase space dominated by the instability. At larger values of $\sigma_{E,i}$, the dependence becomes linear, which reflects the preservation of the longitudinal emittance (Liouvillian behavior), i.e., the instability is largely mitigated or suppressed. On the contrary, the isochronous optics shows σ_{MBI} as being almost independent from $\sigma_{E,i}$ for small values of this parameter (i.e., the non-linear dependence is strongly suppressed), while a linear dependence still exists for larger values.

The final SES is partly reduced by a negative R_{56} value with respect to the positive value (see Table 3), which indicates a contribution of LSC to the total gain. Regardless, the isochronous optics give a 10-fold smaller SES value. In conclusion, the isochronous optics are recommended because they minimize the total gain at the wavelengths of interest and ensure a final phase space that is not modulated by the instability, even for low beam energy spread. With the adopted parameters,

a minimum $\sigma_{E,i} \approx 30$ keV gives an instability level that is largely mitigated when the isochronous optics are implemented. A similar result is obtained for $\sigma_{E,i} > 70$ keV for the non-isochronous optics.

Preservation of the 6-dimensional beam brightness assumes cancellation of the CSR kicks along the switchyard. This is possible with properly tuned linear optics in the bend plane and in the absence of bunch length variation. The latter condition is met at 1 GeV, for example by a beam size of 30 µm at the entrance of the switchyard, and at the same time $\left|R_{51}\right| < 5$ mm^{-1} and $|R_{52}| < 25$ mm; an energy spread of 60 keV implies $|R_{56}| < 2.3$ mm. At the higher beam energy level of 5 GeV, the isochronous optics do not show any relevant modification to the curves in Figures 1 and 2, in confirmation of an instability that is already suppressed at the lower beam rigidity level. The non-isochronous optics show a reduction of the peak gain and of the final slice energy spread by a factor of ~2 with respect to 1 GeV beam energy. The specification for the maximum tolerable value of R_{51} does not change substantially; R_{52} and R_{56} are relaxed by factors of 2 and 5, respectively.

5. Conclusions

An analysis of the MBI in the switchyard following a plasma accelerator is presented, which moves the accelerated electron beam into the undulator for lasing in the soft X-ray range. The study confirms that for state-of-the-art beam parameters at the exit of the plasma cell and for beam energy exceeding 1 GeV, the isochronous optics minimize the MBI along the line, so that minimum degradation of the beam's longitudinal phase space is expected at the undulator entrance. An initial SES energy spread larger than 0.01% promises effective suppression of the instability through Landau damping. The study is limited to the simplified scenario, whereby no phase space modulations accumulate in the accelerator.

Preservation of the bend plane projected emittance from CSR emitted in the switchyard dipole magnets can be achieved under additional constraints on the first-order transport matrix terms of the line. Our findings are further relaxed both in terms of the initial beam parameters and linear optics functions at higher beam energies.

In conclusion, this study confirms the feasibility of beam transport from a state-of-the-art plasma accelerator to an undulator, which is suitable for the preservation of the 6-dimensional beam brightness, and thereby for lasing in the extreme ultra-violet and soft X-ray wavelength ranges.

Author Contributions: Conceptualization and software, S.D.M. and G.P.; formal analysis, G.P.; writing–original draft preparation, S.D.M.; writing–review and editing, S.D.M. and G.P. All authors have read and agreed to the published version of the manuscript.

Funding: This research received no external funding.

Conflicts of Interest: The authors declare no conflict of interest.

References

1. Huang, Z.; Stupakov, G. Control and application of beam microbunching in high brightness linac-driven free electron lasers. *Nucl. Instrum. Phys. Res. A* **2018**, *907*, 182. [CrossRef]
2. Di Mitri, S. Coherent Synchrotron Radiation and Microbunching Instability. In Proceedings of the CERN Accelerator School: Free Electron Lasers and Energy Recovery Linacs, Hamburg, Germany, 31 May–10 June 2016.
3. Saldin, E.L.; Schneidmiller, E.A.; Yurkov, M.V. Klystron instability of a relativistic electron beam in a bunch compressor. *Nucl. Instrum. Phys. Res. A* **2002**, *490*, 1. [CrossRef]
4. Heifets, S.; Stupakov, G.; Krinsky, S. Coherent synchrotron radiation instability in a bunch compressor. *Phys. Rev. Special Topics Accel. Beams* **2002**, *5*, 064401. [CrossRef]
5. Huang, Z.; Kim, K.-J. Formulas for coherent synchrotron radiation microbunching in a bunch compressor chicane. *Phys. Rev. Special Topics Accel. Beams* **2002**, *5*, 074401. [CrossRef]
6. Marcus, G.; Fawley, W.M.; Bohler, D.; Ding, Y.; Feng, Y.; Hemsing, E.; Huang, Z.; Krzywinski, J.; Lutman, A.; Ratner, D. Experimental observations of seed growth and accompanying pedestal contamination in a self-seeded, soft x-ray free-electron laser. *Phys. Rev. Accel. Beams* **2019**, *22*, 080702. [CrossRef]

7. Ratner, D.; Behrens, C.; Ding, Y.; Huang, Z.; Marinelli, A.; Maxwell, T.; Zhou, F. Time-resolved imaging of the microbunching instability and energy spread at the Linac Coherent Light Source. *Phys. Rev. ST Accel. Beams* **2015**, *18*, 030704. [CrossRef]
8. Lu, H.; Liu, M.; Wang, W.; Wang, C.; Liu, J.; Deng, A.; Xu, J.; Xia, C.; Li, W.; Zhang, H.; et al. Laser wakefield acceleration of electron beams beyond 1 GeV from an ablative capillary discharge waveguide. *Appl. Phys. Lett.* **2011**, *99*, 091502. [CrossRef]
9. Wang, W.; Zgadzaj, R.; Fazel, N.; Li, Z.; Yi, S.A.; Zhang, X.; Henderson, W.; Chang, Y.-Y.; Korzekwa, R.; Tsai, H.-E.; et al. Quasi-monoenergetic laser-plasma acceleration of electrons to 2 GeV. *Nat. Commun.* **2013**, *4*, 1988. [CrossRef]
10. Kim, H.T.; Pae, K.H.; Cha, H.J.; Kim, I.J.; Yu, T.J.; Sung, J.H.; Lee, S.K.; Jeong, T.M.; Lee, J. Enhancement of electron energy to the multi-GeV regime by a dual-stage laser-wakefield accelerator pumped by petawatt laser pulses. *Phys. Rev. Lett.* **2013**, *111*, 165002. [CrossRef]
11. Leemans, W.P.; Gonsalves, A.J.; Mao, H.S.; Nakamura, K.; Benedetti, C.; Schroeder, C.B.; Tóth, C.; Daniels, J.; Mittelberger, D.E.; Bulanov, S.S.; et al. Multi-GeV electron beams from capillary-discharge-guided subpetawatt laser pulses in the self-trapping regime. *Phys. Rev. Lett.* **2014**, *113*, 245002. [CrossRef]
12. Maier, A.R.; Meseck, A.; Reiche, S.; Schroeder, C.B.; Seggebrock, T.; Gruner, F. Demonstration scheme for a laser-plasma-driven free-electron laser. *Phys. Rev. X* **2012**, *2*, 031019. [CrossRef]
13. Labat, M.; Loulergue, A.; Andre, T.; Andriyash, I.A.; Ghaith, A.; Khojoyan, M.; Marteau, F.; Valléau, M.; Briquez, F.; Benabderrahmane, C.; et al. Robustness of a plasma acceleration based free electron laser. *Phys. Rev. Accel. Beams* **2018**, *21*, 114802. [CrossRef]
14. André, T.; Andriyash, I.A.; Loulergue, A.; Labat, M.; Roussel, E.; Ghaith, A.; Khojoyan, M.; Thaury, C.; Valléau, M.; Briquez, F.; et al. Control of laser plasma accelerated electrons for light sources. *Nat. Commun.* **2018**, *9*, 1334. [CrossRef]
15. Decking, W.; Obier, F. Layout of the Beam Switchyard at the European XFEL, WEPC073. In Proceedings of the 11th European Particle Accelerator Conference, Genoa, Italy, 23–27 June 2008.
16. Milas, N.; Gough, C. Design of the SwissFEL Switchyard, WEPB16. In Proceedings of the 32nd International Free Electron Laser Conference, Malmö, Sweden, 23–27 August 2010.
17. Placidi, M.; Jung, J.-Y.; Ratti, A.; Sun, C. Compact switchyard schemes. *Nucl. Instr. Meth. Phys. Res. A* **2014**, *768*, 14–19. [CrossRef]
18. Faatz, B.; Plönjes, E.; Ackermann, S.; Agababyan, A.; Asgekar, V.; Ayvazyan, V.; Baark, S.; Baboi, N.; Balandin, V.; Von Bargen, N.; et al. Simultaneous operation of two soft x-ray free-electron lasers driven by one linear accelerator. *New J. Phys.* **2016**, *18*, 062002. [CrossRef]
19. Hara, T.; Fukami, K.; Inagaki, T.; Kawaguchi, H.; Kinjo, R.; Kondo, C.; Otake, Y.; Tajiri, Y.; Takebe, H.; Togawa, K.; et al. Pulse-by-pulse multi-beam-line operation for x-ray free-electron lasers. *Phys. Rev. Accel. Beams* **2016**, *19*, 020703. [CrossRef]
20. Alotaibi, B.M.; Khalil1, S.M.; McNeil, B.W.J.; Traczykowski, P. Modelling a laser plasma accelerator driven free electron laser. *J. Phys. Commun.* **2019**, *3*, 6. [CrossRef]
21. Di Mitri, S.; Cornacchia, M. Electron beam brightness in linac drivers for free-electron-lasers. *Phys. Rep.* **2014**, *539*, 1–48. [CrossRef]
22. Wiggins, S.M.; Issac, R.C.; Welsh, G.H.; Brunetti, E.; Shanks, R.P.; Anania, M.P.; Cipiccia, S.; Manahan, G.G.; Aniculaesei, C.; Ersfeld, B.; et al. High quality electron beams from a laser wakefield accelerator. *Plasma Phys. Contr. Fusion* **2010**, *52*, 12. [CrossRef]
23. Huang, Z.; Ding, Y.; Schroeder, C.B. Compact X-ray free-electron laser from a laser-plasma accelerator using a transverse-gradient undulator. *Phys. Rev. Lett.* **2012**, *109*, 204891. [CrossRef]
24. Samant, S.A.; Upadhyay, A.K.; Krishnagopal, S. High brightness electron beams from density transition laser wakefield acceleration for short-wavelength free-electron lasers. *Plasma Phys. Contr. Fusion* **2014**, *56*, 9. [CrossRef]
25. Pousa, A.F.; de la Ossa, A.M.; Assmann, R. Intrinsic energy spread and bunch length growth in plasma-based accelerators due to betatron motion. *Sci. Rep.* **2019**, *9*, 17690. [CrossRef] [PubMed]
26. Couprie, M.E.; Loulergue, A.; Labat, M.; Lehe, R.; Malka, V. Towards a free electron laser based on laser plasma accelerators. *J. Phys. B* **2014**, *47*, 23. [CrossRef]

27. Brinkmann, R.; Delbos, N.; Dornmair, I.; Kirchen, M.; Assmann, R.; Behrens, C.; Floettmann, K.; Grebenyuk, J.; Gross, M.; Jalas, S.; et al. Chirp mitigation of plasma-accelerated beams by a modulated plasma density. *Phys. Rev. Lett.* **2017**, *118*, 214801. [CrossRef] [PubMed]
28. Pousa, A.F.; de la Ossa, A.M.; Brinkmann, R.; Assmann, R. Compact multistage plasma-based accelerator design for correlated energy spread compensation. *Phys. Rev. Lett.* **2019**, *123*, 054801. [CrossRef] [PubMed]
29. Loulergue, A.; Labat, M.; Evain, C.; Benabderrahmane, C.; Malka, V.; Couprie, M.E. Beam manipulation for compact laser wakefield accelerator based free-electron lasers. *New J. Phys.* **2015**, *17*. [CrossRef]
30. Nghiem, P.A.P.; Assmann, R.; Beck, A.; Chancé, A.; Chiadroni, E.; Cros, B.; Ferrario, M.; Pousa, A.F.; Giribono, A.; Gizzi, L.A.; et al. Toward a plasma-based accelerator at high beam energy with high beam charge and high beam quality. *Phys. Rev. Accel. Beams* **2020**, *23*, 031301. [CrossRef]
31. Bosch, R.A.; Klemann, K.J.; Wu, J. Modeling two-stage bunch compression with wakefields: Macroscopic properties and microbunching instability. *Phys. Rev. ST Accel. Beams* **2008**, *11*, 090702. [CrossRef]
32. Di Mitri, S.; Perosa, G.; Brynes, A.D.; Setija, I.; Spampinati, S.; Williams, P.; Wolski, A.; Allaria, E.; Brussaard, S.; Gianessi, L.; et al. Experimental evidence of intrabeam scattering in a free-electron laser driver. *New J. Phys.* **2020**. [CrossRef]
33. EUPRAXIA Conceptual Design Report. Available online: http://www.lnf.infn.it/sis/preprint/pdf/getfile.php?filename=INFN-18-03-LNF.pdf (accessed on 26 August 2020).
34. Bonifacio, R.; Pellegrini, C.; Narducci, L. Collective instabilities and high-gain regime in a free electron laser. *Opt. Commun.* **1984**, *50*, 373–378. [CrossRef]
35. Venturini, M. Models of longitudinal space-charge impedance for microbunching instability. *Phys. Rev. Spec. Top. Accel. Beams* **2008**, *11*, 034401. [CrossRef]
36. Huang, Z.; Borland, M.; Emma, P.; Wu, J.; Limborg, C.; Stupakov, G.; Welch, J. Suppression of microbunching instability in the linac coherent light source. *Phys. Rev. Spec. Top. Accel. Beams* **2004**, *7*, 074401. [CrossRef]
37. Tsai, C.-Y.; Di Mitri, S.; Douglas, D.; Li, R.; Tennant, C. Conditions for coherent-synchrotron-radiation-induced microbunching suppression in multibend beam transport or recirculation arcs. *Phys. Rev. Accel. Beams* **2017**, *20*, 024401. [CrossRef]
38. Di Mitri, S.; Spampinati, S. Microbunching instability study in a linac-driven free electron laser switchyard beam line. *Phys. Rev. Accel. Beams* **2017**, *20*, 120701. [CrossRef]
39. Perosa, G.; Allaria, E.M.; Badano, L.; Bruchon, N.; Cinquegrana, P.; Danailov, M.B.; Demidovich, A.; De Ninno, G.; Giannessi, L.; Mirian, N.; et al. Linear optics control of sideband instability for improved free-electron laser spectral brightness. *Phys. Rev.* **2020**, in press.
40. Di Mitri, S.; Spampinati, S. Microbunching instability suppression via electron-magnetic-phase mixing. *Phys. Rev. Lett.* **2014**, *112*, 134802. [CrossRef]
41. Derbenev, Y.S.; Rossbach, J.; Saldin, E.L.; Shiltsev, V.D. *Microbunch Radiative Tail—Head Interaction, TESLA-FEL 95-05*; DESY: Hamburg, Germany, 1995.
42. Di Mitri, S.; Cornacchia, M.; Spampinati, S. Cancellation of coherent synchrotron radiation kicks with optics balance. *Phys. Rev. Lett.* **2013**, *110*, 014801. [CrossRef]